frontiers | Frontiers in Earth Science

TYPE Original Research
PUBLISHED 09 January 2023
DOI 10.3389/feart.2022.1035702

OPEN ACCESS

EDITED BY
Qingbang Meng,
China University of Geosciences
Wuhan, China

REVIEWED BY
Jincheng Zhao,
Henan Polytechnic University, China
Junjian Zhang,
Shandong University of Science and
Technology, China

*CORRESPONDENCE
Teng Li,
liteng2052@163.com

SPECIALTY SECTION
This article was submitted to
Geochemistry,
a section of the journal
Frontiers in Earth Science

RECEIVED 03 September 2022
ACCEPTED 13 September 2022
PUBLISHED 09 January 2023

CITATION
Gao Y, Li T, Zhang Z, Yu J, Zhang Y, Li X and Zhao H (2023), Research on fluid mobility in tight-sandstone with a NMR fractal theory pore
classification method.
Front. Earth Sci. 10:1035702.
doi: 10.3389/feart.2022.1035702

Research on fluid mobility in tight-sandstone with a NMR fractal theory pore classification method

Yongli Gao[1], Teng Li[1]*, Zhiguo Zhang[2], Jian Yu[2], Yingke Zhang[2], Xuan Li[3] and Hui Zhao[3]

[1]College of Petroleum Engineering, Xi'an Shiyou University, Xi'an, Shaanxi, China, [2]PetroChina Changqing Oilfield Company, Xi'an, Shaanxi, China, [3]No.2 Oil Production Plant, PetroChina Changqing Oilfield Company, Qingyang, Gansu, China

The fluid mobility characteristics in the pores with various apertures for tight-sandstone would finally determine the fluid mobility and production of tight oil and gas reservoirs. In this study, the tight-sandstone core samples collected from Middle Jurassic Xishanyao Formation in Santanghu Basin were launched the fluid mobility measurements under various centrifugal speeds. With the NMR fractal theory pore classification method, the various types of pores in the tight-sandstone core samples were classified, and the fluid mobility in different types of pores were also investigated. The results show that the tights-sandstone core samples were significantly influenced by compaction, and the core samples are relatively dense, the mineral intergranular solution pores and colloidal intergranular pores are the main storage spaces. With a constant increase of the centrifugal speed, the fluid mobility increases continuously, and the fluid mobility for CTOS-19 features stronger than that of CTOS-7, which is related to the complexity of pore structure in tight-sandstone sample. Compared with the pore aperture in CTOS-19, the pore aperture in CTOS-7 is smaller, and the connectivity between the smaller and larger pores is poorer, leading to the poorer fluid mobility. Besides, the NMR fractal theory pore classification method also shows that the COTS-7 features more pore types than COTS-19, five and four types respectively. The type P2 and P3 pores are dominant in COTS-7 and CTOS-19 core samples, and the connectivity between type P2 and P3 pores contributes dominantly to the fluid mobility. With the NMR fractal theory pore classification method, the complexity of the distribution of fluid and fluid mobility in tight reservoirs could be studied quantitatively, and the results can efficiently guide the development of residual oil and gas in tight oil reservoirs.

KEYWORDS

tight-sandstone, fluid mobility, nuclear magnetic resonance, fractal, pore classification

Introduction

The development of tight-sandstone reservoirs is hot in the field of unconventional oil and gas in recent years. However, the nano-scale pores in the tight oil and gas reservoirs are developed with complex pore structures and strong microscopic heterogeneity. With a refined classification of pores in the tight-sandstone reservoirs, it could ensure the mobility and activation of geological fluids in different scale pore spaces, which would guide the development of tight oil and gas.

Tight-sandstone reservoir features various types, the structure and genesis of pores in tight-sandstone reservoir is complex, and the classification and identification of pores are the basis to study the reservoir characteristics, which is also the core content of reservoir space characterization. Currently, the study of the pores in the tight-sandstone mainly focus on the pore genesis, pore morphology, pore size, pore yield and matrix correlation, etc (Slatt and O'Neal, 2011; Loucks et al., 2012; Yu, 2013). Various measurements have been used to investigate the pore structure of tight-sandstone reservoir, such as scanning electron microscopy (SEM), atomic force microscope (AFM), focus-focused ion beam-electron SEM (FIB-SEM), nano-CT, transmission electron microscope (TEM), high-pressure mercury injection pressure (HMIP), constant-velocity mercury pressure (C-MP), low-temperature nitrogen adsorption (LP-N_2A), low-temperature carbon dioxide adsorption (LP-CO_2A), nuclear magnetic resonance (NMR), small-angle neutron scattering (SANS), small-angle X-ray scattering SAXS, ultra-small angular scattering USAS (Curtis et al., 2012; Javadpour et al., 2012; Melnichenko et al., 2012; Arabjamaloei et al., 2015; Li, 2020, Li et al., 2020; Li et al., 2021a; Li et al., 2021b), and so on.

Nuclear magnetic resonance (NMR) technology, as a nondestructive testing technique, has been widely used in the field of unconventional oil and gas in recent years, such as the fluid distribution characteristics (Mehana and El-Monier, 2016; Lawal et al., 2020; Liu et al., 2020), pore structure (Zhao et al., 2011; Li et al., 2018; Zhang J. et al., 2019; Zhang Q. et al., 2019; Liu et al., 2020; Ma et al., 2020; Wang et al., 2020), seepage characteristics (Sun et al., 2018a; Liu et al., 2020; Wang et al., 2020) and wettability (Sun et al., 2018b; Liu et al., 2020; Mao et al., 2020), etc. NMR technology has unique advantages in characterizing the micro-structural pore features and fluid mobility of reservoirs. Peng et al. (2018) classified the pores of clastic tuffs into micro-pore, small pore, medium pore, and large pore based on the boundary of 30 ms, 90 ms, and 200 ms. Wang et al. (2021) classified the pores in the core of tight reservoirs into completely immobile pores, partially mobile pores, and fully mobile pores based on the mobility of pore fluids. Dai et al. (2019) selected four characteristic points on the NMR T_2 spectrum and classified the pores into nano-pores, small pores, medium pores, and large pores. Li et al. (2022) classified the movable fluid pores in tight cores into four different pore types, P1, P2, P3 and P4 respectively with the fractal method of nuclear magnetic resonance. Based on the combination of multiple methods to form a "wide range, high accuracy, and large scale" pore structure system, which can provide an extremely enrichment pore structure information (Clarkson et al., 2012), such as Gao et al. (2019) used a combination of SEM, HMIP and C-MP to study the pore structure of the pores. In addition, the pore characteristics of tight cores are most widely analyzed by combined HMIP and NMR tests, which convert the NMR transverse relaxation time to pore radius, and this can better determine the quantitative relationship between the NMR transverse relaxation time (T_2) and pore throat radius (Gao and Li, 2015). Commonly, the short peak volume of T_2 distribution corresponds to small pores, and on the basis of pore radium conversion, the pores in tight reservoirs can further be classified into micro-sized large pores (>10 μm), micro-sized micro-pores (1–10 μm). submicro-pores (0.1–1 μm), and nano-pores (<0.1 μm), with submicron pores being the main contributor of movable fluids (Hu et al., 2020).

There have been numerous researches on the classification of pores in the tight-sandstone reservoirs, and the fluid mobility in the tight reservoirs. However, these studies mainly focus on the total fluid mobility in the tight reservoir, and the refined fluid mobility in various types of pores is not studied detailed. In this study, the tight-sandstone core samples of Middle Jurassic Xishanyao Formation in the Santanghu Basin, Norwest China were selected as the subject, and the fluid movable of cores under various centrifugal speeds of saturated simulated water were carried out, combined with the NMR fractal theory pore classification method provided by Li et al. (2022), the types of pores in the tight-sandstones were divided, and quantitatively characterizes the characteristics of fluid movability and the degree of movability in different types of pores were launched.

Experimental materials and experimental test procedures

Experimental materials

The core samples for this study were collected from the Middle Jurassic Xishayao Formation (J_2x) in Santanghu Basin, Northwest China. The tight reservoirs featured strong heterogeneity, and the tight core samples were collected from a nearby region in the full-diameter cores at the horizontal stratification direction. The core samples were polished to ensure that the planeness of the end face was less than 0.01 prior to the measurements. The porosity of the two tight-sandstone samples were extremely low, ranging from 2.72 to 3.97

TABLE 1 The basic information of core samples in this study.

Core no.	Formation	Depth/m	Length/mm	Diameter/mm	Permeability/10^{-3}μm^2	Porosity/%	Pore volume/cm^3
CTOS-7	J_2x	2619.58	25.12	24.62	0.0097	2.72	0.33
CTOS-19		2621.47	25.74	24.52	0.0239	3.97	0.48


项目类别：重点实验室项目

陕西省教育厅
重点科学研究计划项目
合　同　书

项目编号 20JS116
鄂尔多斯盆地东缘上古生界煤系
项目名称 气三节点法合采接替时机研究
项目负责人 李腾
项目起止时间 2020 年 01 月至 2021 年 12 月
陕西省油气田特种增产技术重点
依托平台 实验室
依托单位 西安石油大学

陕西省教育厅印制

FIGURE 1
The SEM photos of the CTOS-7 and CTOS-19 samples. (Yellow zone is the colloidal intergranular pore, green zone is the intergranular solution pores).

%, and the permeability ranging from 0.0097 × 10^{-3} μm^2 to 0.0238 × 10^{-3} μm^2, which are typical extra-low porosity and extra-low permeability reservoirs (Table 1). The test results based on argon ion polishing SEM show that due to the large burial depth, the tight-sandstone samples are compacted tightly and the pores are poorly developed, and the pore types are mainly mineral intergranular solution pores and colloidal intergranular pores, and the developed intergranular solution pores are mostly filled by calcite and clay minerals (Figure 1). The face porosity in CTOS-7 core sample is 3.86 %, while the porosity of intergranular pores in cement contributes almost 78.50 %. As a contrast, the face porosity in CTOS-19 is lower than that of CTOS-7, and the porosity of intergranular pores in cement contributes 67.40 %.

Methods

NMR techniques and fractal theory have unique advantages in characterizing fluid mobility and pore structure features in porous media. In this study, the Oxford Geospec 2/53 NMR high-temperature and high-pressure online displacement system was used to complete the measurements.

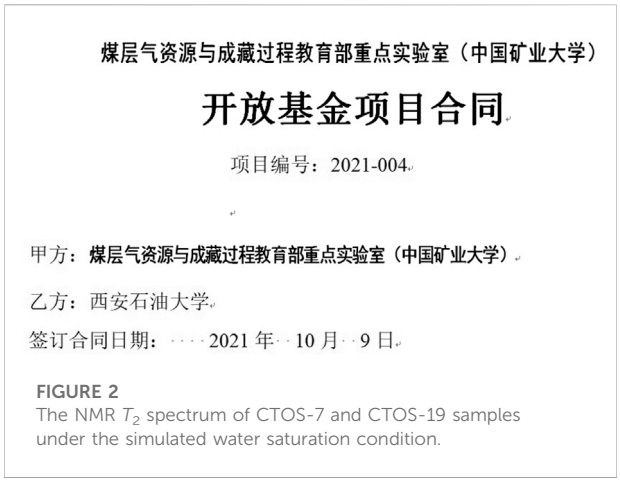
煤层气资源与成藏过程教育部重点实验室（中国矿业大学）

开放基金项目合同

项目编号：2021-004

甲方：煤层气资源与成藏过程教育部重点实验室（中国矿业大学）

乙方：西安石油大学

签订合同日期：2021 年 10 月 9 日

FIGURE 2
The NMR T_2 spectrum of CTOS-7 and CTOS-19 samples under the simulated water saturation condition.

The specific NMR testing procedures for fluid mobility of tight cores at different centrifugal speeds are as follows: 1) the oil-washed small-diameter cores were dried in a drying oven at 80°C for 48 h, and the porosity and permeability of the dried cores were tested; 2) the dried cores were saturated in a NM-V vacuum pressurized saturation device for 48 h to ensure that the cores were completely saturated with simulated water, and the saturated cores would be scanned by the NMR system; 3) the saturated cores would be put in a centrifuge and centrifuged at 1,300 r/min for 30 min, and then scanned the cores with NMR T_2 spectra; 4) repeat step 2 and complete centrifugation at 3,000 r/min, 4,200 r/min, 6,000 r/min and 8,500 r/min respectively.

The NMR relaxation time includes three parts, surface relaxation time, fluid relaxation time and molecular diffusion relaxation time. However, the latter two are usually ignored, and the surface relaxation time is often used to approximately characterize the transverse relaxation time of porous media (Kenyon et al., 1988; Howard et al., 1993; Guo and Kantzas, 2009). Combined with the fractal theory, the pore fractal characterization of porous media based on NMR can be realized,

$$\lg(S_v) = (3 - D)lgT_2 + (D - 3)lgT_{2max} \quad (1)$$

where S_v is the cumulative volume fraction of pores with aperture below r; D is the pore fractal dimension of pores with aperture below r; T_2 is the transverse relaxation time corresponding to pore radius r, ms; T_{2max} is the maximum transverse relaxation time, ms.

Based on the NMR fractal theory pore classification method provided by Li et al. (2022), the types of pores in the cores would firstly divided with a fractal dimension of 2, and then the pore fractal dimension correlation coefficient mutation point is used as the secondary pore classification point for the classified primary pore classification,

$$R^{2'} = \frac{R_{i+1}^2 - R_i^2}{R_i^2} \quad (2)$$

where R_i^2 is the correlation coefficient between lg (T_{2i}) and lg (S_{vi}) *at* T_{2i}; R_{i+1}^2 is the correlation coefficient between lg (T_{2i+1}) and lg (S_{vi+1}) *at* T_{2i+1}.

Based on this, the pore classification of porous media with the NMR fractal theory pore classification method is completed.

Results

Fluid distribution characteristics in the core under saturated water condition

The simulated water saturation experiments were carried out with two core samples using an ultra-vacuum saturation device. For the two samples, the simulated water showed a three-peak pattern distribution in the cores, and the left peak patters was higher than the middle peak, and significantly higher than the right one (Figure 2). Previous studies have shown that the distribution characteristics of fluids in NMR T_2 spectra of porous media are closely related to the distribution characteristics of pores at various scales, and the smaller lateral relaxation times tend to correspond to smaller-scale pores in porous media. Accordingly, it can be seen that the pores in CTOS-7 and CTOS-19 are dominated by smaller-scale pores and supplemented by larger-scale pores, in addition to the development of a certain number of micro-fractures in the cores. However, it is worth noticing that the smaller-scale pores in COTS-7 occupy the absolute dominant position, and the larger-scale pores in CTOS-7 are significantly less than those in CTOS-19. In addition, the rapid decrease of lateral duration in CTOS-7 at T_2 = 4 ms and T_2 = 100 ms also reflect the poor connectivity among its smaller-scale pores, larger-scale pores and micro-fractures. This also determines, to some extent, that the fluid mobility in CTOS-7 is worse than that in COTS-19.

Characteristics of movable fluid with different centrifugal speeds

Centrifugal tests were carried out at five different speeds of 1,300 r/min, 3,000 r/min, 4,200 r/min, 6,000 r/min and 8,500 r/min to understand the characteristics of movable fluids in the tight-sandstone samples at different speeds (Figure 3). This is mainly related to the low distribution in the larger-scale pores and micro-fractures in the samples. With the continuous increase of centrifugal speed, the percent movable fluid in CTOS-7 slowly increases to 7.81 %, while the percent movable fluid in CTOS-19 rapidly increases to 23.59 % (Figure 4). For CTOS-7, the fluid in the small amount of developed micro-fractures decreases rapidly,

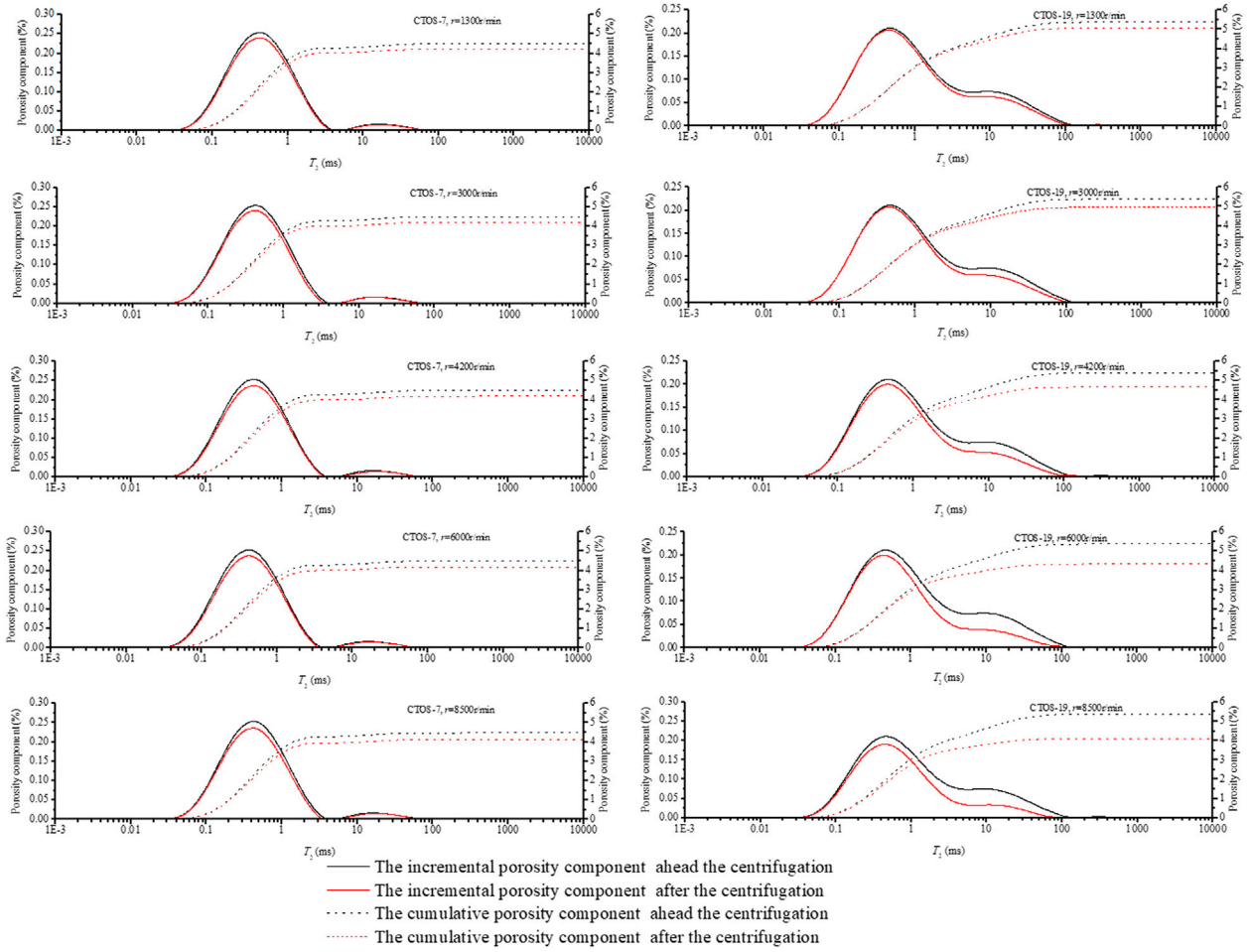

FIGURE 3
The NMR T_2 spectrum of CTOS-7 and CTOS-19 samples under various centrifugal speeds.

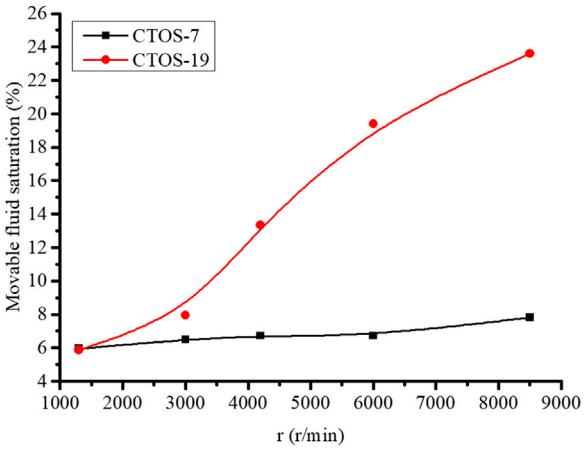

FIGURE 4
The movable fluid saturation of CTOS-7 and CTOS-19 samples under various centrifugal speeds.

and the fluid in the larger-scale pores hardly decreases due to the poor connectivity of pores, while the simulated water in the smaller pores also decreases a little. For CTOS-19 with more developed larger-scale pores, the simulated water in the micro-fractures and larger-scale pores decreased rapidly at small centrifugal speeds, and the simulated water in the smaller-scale pores begins to decrease continuously as the centrifugal speed continues to increase.

Discussion

Classification of pore types in tight-sandstone samples

The pore structure of porous media has typical fractal characteristics. With the NMR fractal theory pore classification method proposed by Li et al. (2022), the pores

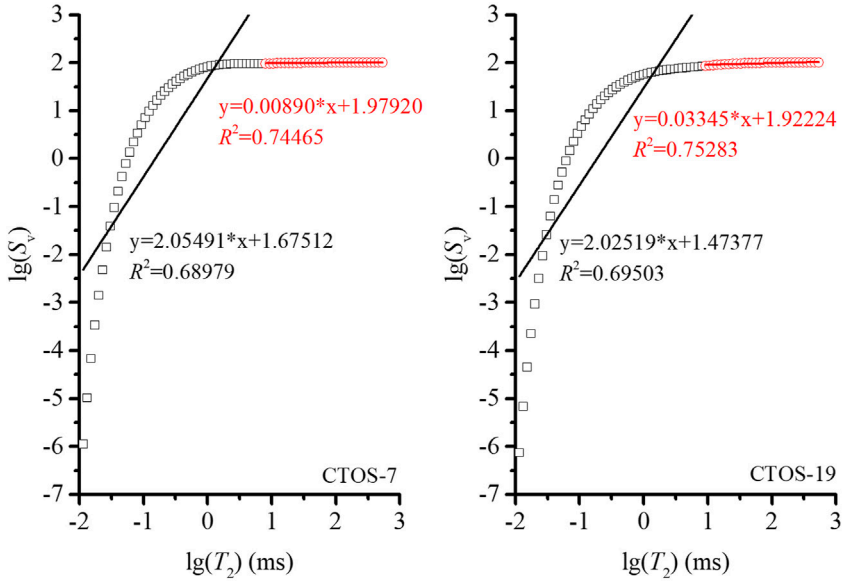

FIGURE 5
The primary pore classification of CTOS-7 and CTOS-19 samples.

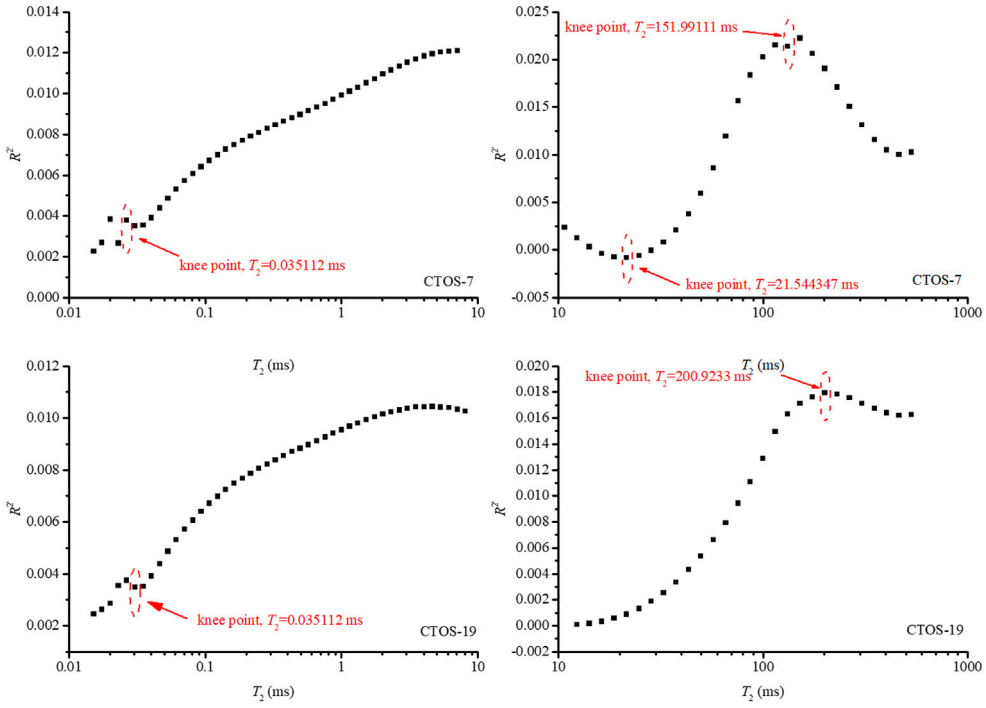

FIGURE 6
The secondary pore classification of CTOS-7 and CTOS-19 samples.

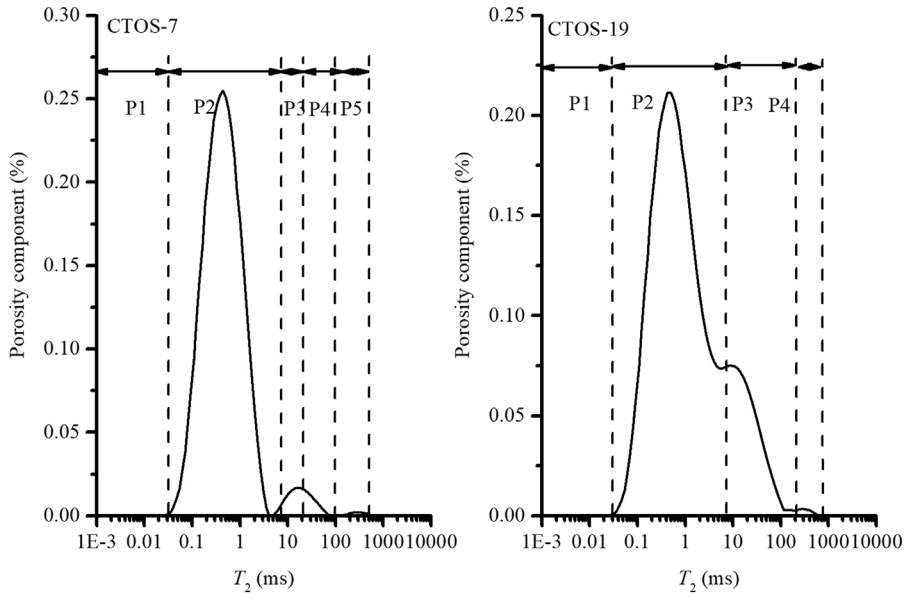

FIGURE 7
The various types of pores in CTOS-7 and CTOS-19 samples.

TABLE 2 The ratio of various types of pore in CTOS-7 and CTOS-19 samples.

Pore types	Ratio/%	
	CTOS-7	CTOS-19
P1	0.01	0.01
P2	39.91	53.13
P3	15.20	23.61
P4	27.27	23.25
P5	17.61	—

in CTOS-7 and CTOS-19 can be roughly divided into two segments with T_2 = 7.054802 ms and T_2 = 8.111,308 ms (Figure 5). On this basis, the T_2 value with the greatest variation in pore of the two previously divided sections was searched for on the principle of the greatest variation in adjacent variability. For CTOS-7, the pores distributed in the interval of T_2 < 7.054802 ms can be further divided into two different types of pores at T_2 = 0.035112 ms; while the pores distributed in the interval of $T_2 \geq 7.054802$ ms, bounded by T_2 = 21.544,347 ms and T_2 = 151.99111 ms, can be further divided into the part of pores can be further divided into three different types of pores (Figure 6). As for CTOS-19, the pores distributed in the interval of T_2 < 8.11308 ms can be further classified into two different types of pores at T_2 = 0.035112 ms; while the pores distributed in the interval of $T_2 \geq 8.11308$ ms can be further classified into two different types of pores with the boundary of T_2 = 200.9233 ms for this part of pores (Figure 6).

Based on the above pore classification principles, the pores in CTOS-7 are divided into five types, among which the type P2 pores are the main type, with a small number of P2 and P4 types pores, and a very small number of P5 type pores, while P1 type pores are almost undeveloped. The P2 type pore is also the main pore type in CTOS-19, followed by P3 type pore, a few P4 pores are developed, and P1 type pore is also not developed (Figure 7; Table 2).

Fractal characteristics of different types of pores

The pore fractal dimension of CTOS-7 shows a gradual increase in pore complexity as the pore radius increases, and the pore fractal dimension of the three different pore type P3, P4 and P5 are all higher, 2.97433, 2.99467 and 2.99727 respectively. The pore fractal characteristics for CTOS-19 are similar to CTOS-7. The pore fractal dimension of CTOS-7 and CTOS-19 with saturated water shows that the pore structure of larger pore is significantly more complex than that of smaller pore (Figure 8; Table 3).

The variability between different types of pore fractal dimension can also be reflected, to some extent, the connectivity between different scales of pores within a porous medium, which will further determine the connectivity of pores in a porous medium. In order to quantitatively characterize the

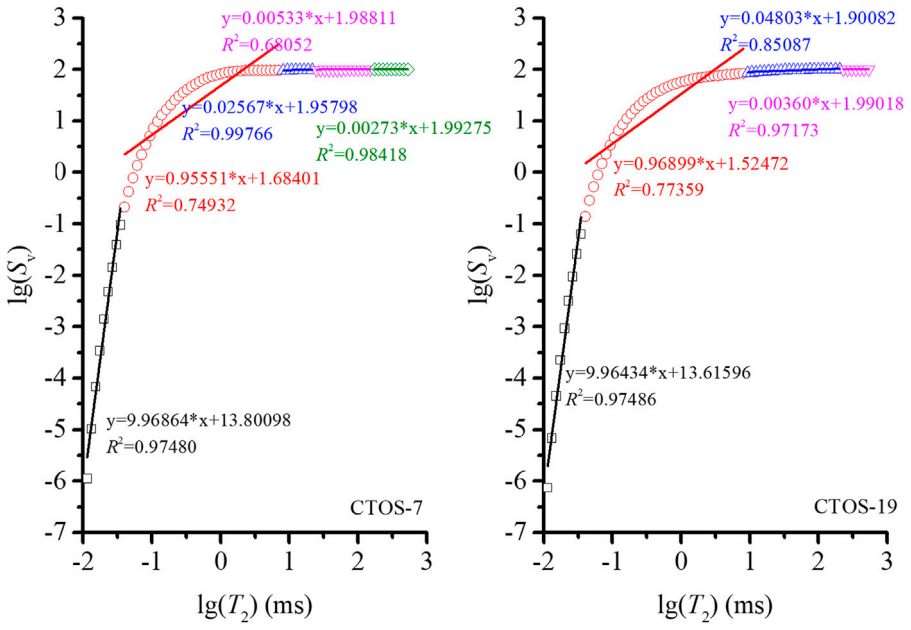

FIGURE 8
The pore fractal dimension of various pores in CTOS-7 and CTOS-19 samples.

TABLE 3 The fractal dimensions of various type of pore in CTOS-7 and CTOS-19 samples.

Pore types	Fractal dimension	
	CTOS-7	CTOS-19
P1	—	—
P2	2.04449	2.03101
P3	2.97433	2.95197
P4	2.99467	2.9964
P5	2.99727	—

variability of fractal dimension between different types of pores, d_p is introduced to characterize it.

$$dp = (Di + 1 - Di)/Di \quad (3)$$

where d_p is the difference index of adjacent pore types; D_i is the pore fractal dimension of the ith type of pore.

The d_p of COTS-7 is 0.4548 for P2 and P3 type pores, 0.0068 for P3 and P4 type pore, and 0.0026 for P4 and P5 type pore. It can be seen that as the pore size in tight-sandstone sample gradually increases, the connectivity between larger size pores is increasing, while the difference between smaller size pores and larger size pores is greater. The d_p of COTS-19 is 0.4534 for P2 and P3 type pores and 0.0151 for P3 and P4 type pore, and the variation pattern of pore difference index among different types of pores is consistent with that of CTOS-7. It is noteworthy that the pore variability index of P3 and P4 types in CTOS-19 is higher than that in CTOS-7, while the pore variability index of P2 and P3 types shows the opposite characteristics, and P2 and P3 types pores are the main pore types in both samples. Combining the fluid mobility characteristics of CTOS-7 and CTOS-19, it is clear that the fluid mobility characteristics of tight-sandstone samples are mainly controlled by both the number of major pore types and pore variability, especially the pore variability between major pore types, and the smaller the variability of major pore types, the better pore fluid mobility can be obtained.

The pore fractal dimension of different types of pores in the tight-sandstone sample will change dynamically as the centrifugal speed increases,. The fractal dimension of P3, P4 and P5 type pores hardly changed for CTOS-7, which also implies that the discharge of fluid from P2 type pore is the key to the increase of fluid mobility. The pore fractal dimension of P2 increases with the increase of centrifugal speed, while that for P3 pores is S-shaped in CTOS-19, and the pore (Figure 9). The continued discharge of fluids from simple pores in the P3 type pore leads to further strengthening of the remaining fluids by capillary action of more complex pore structures, which is the reason for the gradual increase of pore fractal dimension of P3 type pore. The decrease of the pore fractal dimension of the P2 type pore is mainly due to the discharge of fluids in pores more similar to the P3 type pore, and then the discharge of fluids bound by capillary forces leads to the increase of the pore fractal dimension.

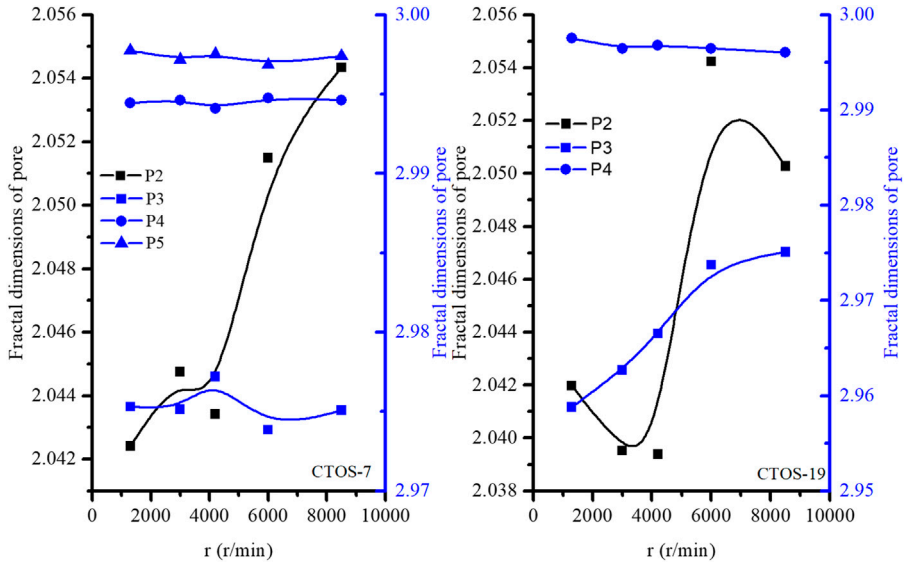

FIGURE 9
The difference change of pore fractal dimension for various pores in CTOS-7 and CTOS-19 samples.

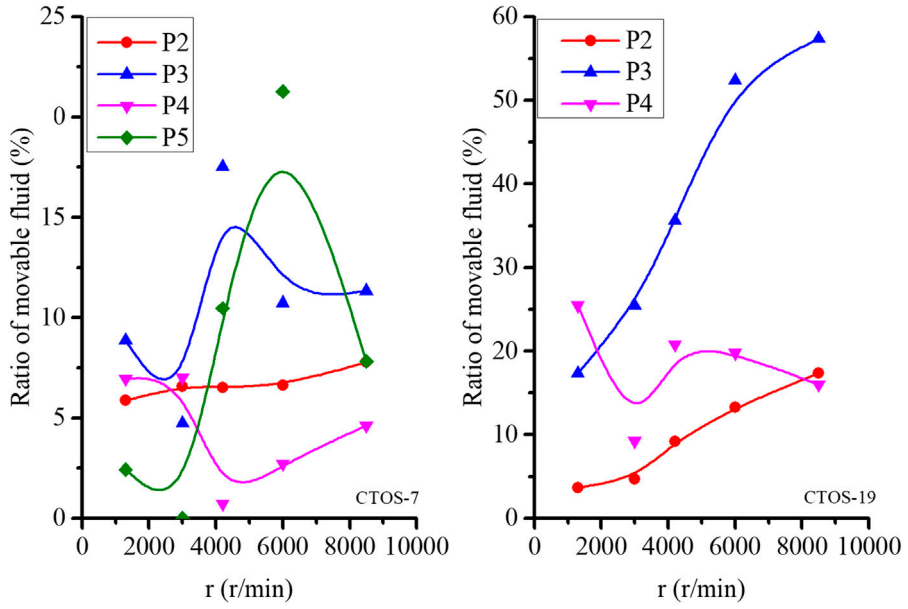

FIGURE 10
The difference mobility of fluids in various pores of CTOS-7 and CTOS-19 samples.

Characteristics of fluid mobility in different types of pores

It can be found that P2 type pore are dominant in COTS-7, and the pore structure complexity of P2 type pores is much smaller that other types of pores. However, due to the poor connectivity between P2 and P3 type pores, CTOS-7 can discharge less fluid through the centrifugation process. P2 and P3 type pores are the main pores in CTOS-19, the better pore connectivity of P2 and P3 pore types leads to the continuous linear discharge of fluids from those two types of pores. In addition, the larger pore size of P3 type pore also contributes to the rapid and large discharge of fluid from those types of pores (Figure 10).

Characteristics of pore fluid different mobility in different types of tight-sandstone samples

The two tight-sandstone samples used in this study are dominated by smaller size pore, but the typical pore development characteristics of the two samples determine significantly different fluid mobility characteristics. The predominance of small size pores and the poor pore connectivity between small size pores and larger size pores lead to a variety of pore types in the cores on the one hand, and poor connectivity between smaller size pores and larger size pores on the other hand, which ultimately leads to the inability of the fluid deposited in the smaller size pores to drain quickly. Further, fluid mobility is mainly controlled by the volume of the main pore types developed in the tight-sandstone and the connectivity between them.

Conclusion

1) The increase of centrifugal speed can effectively improve the fluid mobility in tight-sandstone sample. However, the pore structure connectivity within the tight-sandstone sample is the key to determine the fluid mobility, especially the connectivity between the main reservoir spaces of fluid deposits in the tight-sandstone.
2) The NMR fractal theory pore classification method can better reflect the complexity of pores in tight-sandstone. The more pore types, the stronger the pore complexity of the tight-sandstone, and the poorer the fluid mobility. In addition, the fluid discharge is extremely restricted in tight-sandstone with complex pore structure and poor pore connectivity.
3) In the process of gradual discharge of fluids, the pore fractal dimension of the main pore where fluids are endowed also shows a gradual increase, which is mainly the result of the capillary force of the remaining fluids by the complex pore structure.

Data availability statement

The data analyzed in this study is subject to the following licenses/restrictions: The data could be used when all of the authors agree that requests to access these datasets should be directed to liteng2052@163.com.

Author contributions

YG, ZZ, JY, and YZ completed the field data acquisition. TL completed the data analyses, and wrote the article. XL and HZ complete the measurements. All authors have read and agreed to the published version of the manuscript.

Funding

This work was supported by Scientific Research Program Funded by Shaanxi Provincial Education Department (Program No. 20JS116), and Key Laboratory of Coalbed Methane Resources and Reservoir Formation Process of Ministry of Education (China University of Mining and Technology) (Program No. 2021-004).

The authors declare that this study received funding from PetroChina. The funder was not involved in the study design, collection, analysis, interpretation of data, the writing of this article, or the decision to submit it for publication.

Acknowledgments

The writing and structure of manuscript was supported by Hai Huang.

Conflict of interest

ZZ, JY, YZ, XL, and HZ were employed by the Company PetroChina Changqing Oilfield Company.

The remaining authors declare that the research was conducted in the absence of any commercial or financial relationships that could be construed as a potential conflict of interest.

Publisher's note

All claims expressed in this article are solely those of the authors and do not necessarily represent those of their affiliated organizations, or those of the publisher, the editors and the reviewers. Any product that may be evaluated in this article, or claim that may be made by its manufacturer, is not guaranteed or endorsed by the publisher.

References

Arabjamaloei, R., Ruth, D. W., Mason, G., and Morrow, N. R. (2015). Solutions for countercurrent spontaneous imbibition as derived by means of a similarity approach. *J. Porous Media* 18 (2), 113–124. doi:10.1615/JPorMedia.v18.i2.30

Clarkson, C. R., Freeman, M., He, L., Agamalian, M., Melnichenko, Y. B., Mastalerz, M., et al. (2012). Characterization of tight gas reservoir pore structure using USANS/SANS and gas adsorption analysis. *Fuel* 95, 371–385. doi:10.1016/j.fuel.2011.12.010

Dai, C., Cheng, R., Sun, X., Liu, Y., Zhou, H., Wu, Y., et al. (2019). Oil migration in nanometer to micrometer sized pores of tight oil sandstone during dynamic surfactant imbibition with online NMR. *Fuel* 245, 544–553. doi:10.1016/j.fuel.2019.01.021

Gao, H., Cao, J., Wang, C., He, M., Dou, L., Huang, X., et al. (2019). Comprehensive characterization of pore and throat system for tight sandstone reservoirs and associated permeability determination method using SEM, rate-controlled mercury and high pressure mercury. *J. Pet. Sci. Eng.* 174, 514–524. doi:10.1016/j.petrol.2018.11.043

Gao, H., and Li, H. (2015). Determination of movable fluid percentage and movable fluid porosity in ultra-low permeability sandstone using nuclear magnetic resonance (NMR) technique. *J. Pet. Sci. Eng.* 133, 258–267. doi:10.1016/j.petrol.2015.06.017

Guo, R., and Kantzas, A. (2009). Assessing the water uptake of Alberta coal and the impact of CO_2 injection with low-field NMR. *J. Can. Pet. Technol.* 48 (7), 40–46. doi:10.2118/09-07-40

Howard, J. J., Kenyon, W. E., and Straley, C. (1993). Proton-magnetic resonance and pore-size variations in reservoir sandstones. *SPE Form. Eval.* 8 (3), 194–200. doi:10.2118/20600-PA

Hu, Y., Guo, Y., Shangguan, J., Zhang, J., and Song, Y. (2020). Fractal characteristics and model applicability for pores in tight gas sandstone reservoirs: A case study of the upper paleozoic in ordos basin. *Energy fuels.*. 34 (12), 16059–16072. doi:10.1021/acs.energyfuels.0c03073

Kenyon, W. E., Day, P. I., Straley, C., and Willemsen, J. F. (1988). A three part study of NMR longitudinal relaxation properties of water-saturated sandstones. *SPE Form. Eval.* 3 (3), 622–636. doi:10.2118/15643-PA

Lawal, L. O., Adebayo, A. R., Mahmoud, M., Dia, B. M., and Sultan, A. S. (2020). A novel NMR surface relaxivity measurements on rock cuttings for conventional and unconventional reservoirs. *Int. J. Coal Geol.* 231, 103605. doi:10.1016/j.coal.2020.103605

Li, T., Gao, H., Wang, C., Cheng, Z., Xue, J., Zhang, Z., et al. (2022). Oil utilization degree at various pore sizes via different displacement methods. *J. Pet. Explor. Prod. Technol.* 12 (8), 2271–2287. doi:10.1007/s13202-022-01464-7

Li, T. (2020). The dynamic change of pore structure for the low-rank coal with various pretreatment temperatures: A case study from southwestern ordos basin. *Geofluids* 2020, 1–13. doi:10.1155/2020/8879742

Li, T., Wu, C. F., and Wang, Z. W. (2021a). The dynamic change of pore structure for low-rank coal under refined upgrading pretreatment temperatures. *Pet. Sci.* 18, 430–443. doi:10.1007/s12182-020-00536-9

Li, T., Wu, C., and Wang, Z. (2020). Isothermal characteristics of methane adsorption and changes in the pore structure before and after methane adsorption with high-rank coal. *Energy Explor. Exploitation* 38 (5), 1409–1427. doi:10.1177/0144598720925979

Li, T., Wu, J. J., Wang, X. G., and Huang, H. (2021b). Particle size effect and temperature effect on the pore structure of low-rank coal. *Acs Omega* 6 (8), 5865–5877. doi:10.1021/acsomega.0c06280

Li, Z., Shen, X., Qi, Z., and Hu, R. (2018). Study on the pore structure and fractal characteristics of marine and continental shale based on mercury porosimetry, N_2 adsorption and NMR methods. *J. Nat. Gas. Sci. Eng.* 53, 12–21. doi:10.1016/j.jngse.2018.02.027

Liu, Z., Liu, D., Cai, Y., Yao, Y., Pan, Z., and Zhou, Y. (2020). Application of nuclear magnetic resonance (NMR) in coalbed methane and shale reservoirs: A review. *Int. J. Coal Geol.* 218, 103261. doi:10.1016/j.coal.2019.103261

Loucks, R. G., Reed, R. M., Ruppel, S. C., and Hammes, U. (2012). Spectrum of pore types and networks in mudrocks and a descriptive classification for matrix-related mudrock pores. *Am. Assoc. Pet. Geol. Bull.* 96 (6), 1071–1098. doi:10.1306/08171111061

Ma, X., Wang, H., Zhou, S., Feng, Z., Liu, H., and Guo, W. (2020). Insights into NMR response characteristics of shales and its application in shale gas reservoir evaluation. *J. Nat. Gas. Sci. Eng.* 84, 103674. doi:10.1016/j.jngse.2020.103674

Mao, Y., Xia, W., Peng, Y., and Xie, G. (2020). Wetting of coal pores characterized by LF-NMR and its relationship to flotation recovery. *Fuel* 272, 117737. doi:10.1016/j.fuel.2020.117737

Mehana, M., and El-monier, I. (2016). Shale characteristics impact on Nuclear Magnetic Resonance (NMR) fluid typing methods and correlations. *Petroleum* 2 (2), 138–147. doi:10.1016/j.petlm.2016.02.002

Melnichenko, Y. B., He, L., Sakurovs, R., Kholodenko, A. L., Blach, T., Mastalerz, M., et al. (2012). Accessibility of pores in coal to methane and carbon dioxide. *Fuel* 91, 200–208. doi:10.1016/j.fuel.2011.06.026

Peng, Y., Zhou, C., Fan, Y., Li, C., Yuan, C., and Cong, Y. (2018). A new permeability calculation method using nuclear magnetic resonance logging based on pore sizes: A case study on bioclastic limestone reservoirs in the A oilfield of the mid-ease. *Pet. explor. Dev.* 45 (1), 183–192. doi:10.1016/S1876-3804(18)30019-3

Slatt, E. M., and O'Neal, N. R. (2011). Pore types in the Barnett and Woodford gas shales: Contribution to understanding gas storage and migration pathways in fine-grained rocks. *Am. Assoc. Pet. Geol. Bull.* 95 (12), 2017–2030. doi:10.1306/03301110145

Sun, X., Yan, Y., Ripepi, N., and Liu, D. (2018a). A novel method for gas-water relative permeability measurement of coal using NMR relaxation. *Transp. Porous Med.* 124, 73–90. doi:10.1007/s11242-018-1053-y

Sun, X., Yao, Y., Liu, D., and Zhou, Y. (2018b). Investigations of CO_2-water wettability of coal: NMR relaxation method. *Int. J. Coal Geol.* 188, 38–50. doi:10.1016/j.coal.2018.01.015

Wang, F., Zeng, F., Wang, L., Hou, X., Cheng, H., and Gao, J. (2021). Fractal analysis of tight sandstone petrophysical properties in unconventional oil reservoirs with NMR and rate-controlled porosimetry. *Energy fuels.* 35 (5), 3753–3765. doi:10.1021/ACS.ENERGYFUELS.0C03394

Wang, G., Han, D., Qin, X., Liu, Z., and Liu, J. (2020). A comprehensive method for studying pore structure and seepage characteristics of coal mass based on 3D CT reconstruction and NMR. *Fuel (Lond).* 281, 118735. doi:10.1016/j.fuel.2020.118735

Yu, B. S. (2013). Classification and characterization of gas shale pore system. *Earth Sci. Front.* 20 (4), 211–220.

Zhang, J., Wei, C., Ju, W., Yan, G., Lu, G., Hou, X., et al. (2019a). Stress sensitivity characterization and heterogeneous variation of the pore-fracture system in middle-high rank coals reservoir based on NMR experiments. *Fuel* 238, 331–344. doi:10.1016/j.fuel.2018.10.127

Zhang, Q., Dong, Y., Liu, S., Elsworth, D., and Zhao, Y. (2019b). Shale pore characterization using NMR cryoporometry with octamethylcyclotetrasiloxane as the probe liquid. *Energy fuels.* 31 (7), 6951–6959. doi:10.1021/acs.energyfuels.7b00880

Zhao, Y., Sun, Y., Liu, S., Wang, K., and Jiang, Y. (2011). Pore structure characterization of coal by NMR cryoporometry. *Fuel* 190, 359–369. doi:10.1016/j.fuel.2016.10.121